Inorg. Chem. **2008**, *47*, 7824−7833

Covalency in the f Element−Chalcogen Bond. Computational Studies of $M[N(EPR_2)_2]_3$ (M = La, Ce, Pr, Pm, Eu, U, Np, Pu, Am, Cm; E = O, S, Se, Te; R = H, ^{i}Pr, Ph)

Kieran I. M. Ingram,[†] Matthew J. Tassell,[†] Andrew J. Gaunt,[‡] and Nikolas Kaltsoyannis*[,†]

Department of Chemistry, University College London, 20 Gordon Street, London WC1H 0AJ, U.K., and Chemistry Division, Los Alamos National Laboratory, Los Alamos, New Mexico 87545

Received May 7, 2008

The geometric and electronic structures of the title complexes have been studied using scalar relativistic, gradient-corrected density functional theory. Extension of our previous work on six-coordinate $M[N(EPH_2)_2]_3$ (M = La, Ce, U, Pu; E = O, S, Se, Te), models for the experimentally characterized $M[N(EP^iPr_2)_2]_3$, yields converged geometries for all of the other 4f and 5f metals studied and for all four group 16 elements. By contrast, converged geometries for nine-coordinate $M[N(EPPh_2)_2]_3$ are obtained only for E = S and Se. Comparison of the electronic structures of six- and nine-coordinate $M[N(EPH_2)_2]_3$ suggests that coordination of the N atoms produces only minor changes in the metal−chalcogen interactions. Six-coordinate $Eu[N(EPH_2)_2]_3$ and $Am[N(EPH_2)_2]_3$ with the heavier group 16 donors display geometric and electronic properties rather different from those of the other members of the 4f and 5f series, in particular, longer than expected Eu−E and Am−E bond lengths, smaller reductions in charge difference between M and E down group 16, and larger f populations. The latter are interpreted not as evidence of f-based metal−ligand covalency but rather as being indicative of ionic metal centers closer to M^{II} than M^{III}. The Cm complexes are found to be very ionic, with very metal-localized f orbitals and Cm^{III} centers. The implications of the results for the separation of the minor actinides from nuclear wastes are discussed, as is the validity of using La^{III}/U^{III} comparisons as models for minor actinide/Eu systems.

Introduction

Typical ligands for actinide atoms in coordination compounds have traditionally been based around hard donors, most notably oxygen. However, the chemistry of the actinides with softer donors has not gone unexplored,[1–8] facilitating the assessment of the ability of the 5f elements to engage in covalent bonding. These studies are motivated partly by fundamental interest but also by a desire to provide a chemical bonding rationale for separating An^{III} ions from Ln^{III} ions of similar ionic radii, an important problem that needs to be addressed in advanced nuclear fuel cycles.[9–15] More specifically, it is highly desirable to be able to selectively extract the so-called minor actinides (Am and Cm)

* To whom correspondence should be addressed. E-mail: n.kaltsoyannis@ucl.ac.uk.
† University College London.
‡ Los Alamos National Laboratory.

(1) Brennan, J. G.; Stults, S. D.; Andersen, R. A.; Zalkin, A. *Organometallics* **1988**, *7*, 1329.
(2) Mazzanti, M.; Wietzke, R.; Pécaut, J.; Latour, J.-M.; Maldivi, P.; Remy, M. *Inorg. Chem.* **2002**, *41*, 2389.
(3) Karmazin, L.; Mazzanti, M.; Pécaut, J. *Chem. Commun.* **2002**, 654.
(4) Guillaumont, D. *J. Phys. Chem. A* **2004**, *108*, 6893.
(5) Gaunt, A. J.; Scott, B. L.; Neu, M. P. *Chem. Commun.* **2005**, 3215.
(6) Gaunt, A. J.; Scott, B. L.; Neu, M. P. *Angew. Chem., Int. Ed.* **2006**, *45*, 1638.
(7) Ingram, K. I. M.; Kaltsoyannis, N.; Gaunt, A. J.; Neu, M. P. *J. Alloys Compd.* **2007**, *444*−*445*, 369.
(8) Gaunt, A. J.; Reilly, S. D.; Enriquez, A. E.; Scott, B. L.; Ibers, J. A.; Sekar, P.; Ingram, K. I. M.; Kaltsoyannis, N.; Neu, M. P. *Inorg. Chem.* **2008**, *47*, 29.
(9) Choppin, G. R.; Nash, K. L. *Radiochim. Acta* **1995**, *70*−*1*, 225.
(10) Madic, C.; Hudson, M. J. *High-Level Liquid Waste Partitioning by Means of Completely Incinderable Extractants*; European Commission: Luxembourg, 1998; EUR 18038.
(11) Madic, C.; Hudson, M. J.; Liljenzin, J.-O.; Glatz, J.-P.; Nannicini, R.; Facchini, A.; Kolarik, Z.; Odoj, R. *New Partitioning Techniques for Minor Actinides*; European Commission: Luxembourg, 2000; EUR 19149.
(12) Madic, C.; Testard, F.; Hudson, M. J.; Liljenzin, J.-O.; Christiansen, B.; Ferrando, M.; Facchini, A.; Geist, A.; Modolo, G.; Gonzales-Espartero, A.; De Mendoza, J. *PARTNEW*−*New Solvent Extraction Processes for Minor Actinides*; Commissariat à l'Energie Atomique: Gif sur Yvette Cedex, France, 2004; CEA-R-6066.
(13) Jensen, M. P.; Bond, A. H. *Radiochim. Acta* **2002**, *90*, 205.
(14) Jensen, M. P.; Bond, A. H. *J. Am. Chem. Soc.* **2002**, *124*, 9870.
(15) Andrae, D.; Haeussermann, U.; Dolg, M.; Stoll, H.; Preuss, H. *Theor. Chim. Acta* **1990**, *77*, 123.

10.1021/ic800835k CCC: $40.75
Published on Web 07/26/2008

from the lanthanides, in order to reprocess them into fuel and transmute them in reactors in order to minimize the quantities of highly radioactive waste and to reduce the length of time that it must be stored in geological repositories. One possible approach to developing this technology is to employ extractant ligands that exploit the greater tendency of the 5f elements to engage in covalent bonding.

We recently published a combined experimental and computational study of $M[N(EPR_2)_2]_3$ complexes, with the aim of probing differences in the metal−ligand bond as a function of both metal and donor atoms.[7,8] Experimentally, the systems studied featured M = U, Pu, La, and Ce, with S-, Se-, and Te-based ligands and with R = Ph, ^{i}Pr. Computationally, we chose to model the ^{i}Pr complexes of all four metals, replacing ^{i}Pr with H and studying all E from O to Te. We showed that the U−E bonds are shorter than the corresponding La−E bonds to a significantly larger extent than the difference in the ionic radii between U^{III} and La^{III} and that the same is true between Pu^{III} and Ce^{III}, consistent with increased covalency in actinide bonding. The magnitude of this difference was found to be larger, the softer the donor atom (Te > Se > S), again consistent with enhanced covalency, and computational analysis supported the structural conclusions in finding greater covalency in the actinide complexes with the heavier chalcogen donors.

An important conclusion from the computational study was that the enhanced covalency in the Pu−E complexes (vs analogous Ce^{III} systems) as group 16 is descended, although slightly less than that in the analogous U/La compounds, is still significant. This is important because it is not unequivocally established that the U^{III}/La^{III} comparison is a valid model for that between the trivalent minor actinides and other Ln^{III}. The radiological hazards of working with Am and Cm, and the scarcity of suitable precursors, are such that comparisons based on earlier actinides are often the only way in which extensive progress can be made experimentally, and it was interesting to observe that the An^{III}/Ln^{III} differences hold up when moving to the right in the 4f (Ce) and 5f (Pu) series.

In this contribution, we extend our computational study of $M[N(EPH_2)_2]_3$ to include Pr, Pm, and Eu in the 4f series and Np, Am, and Cm among the actinides to establish if the differences between the early actinides and lanthanides remain in the middle of each series. We focus particularly on the minor actinides and Eu because this comparison is the one most often reported. Furthermore, our previous computational study focused solely on models for the experimental ^{i}Pr ligands. Synthetically, these ligands yield six-coordinate complexes in which each ligand binds in a bidentate manner through its two chalcogen atoms. By contrast, substituting ^{i}Pr by Ph leads to tridentate ligands and nine coordination because each ligand additionally binds through its N atoms. In this paper, we extend our study to encompass the Ph-based ligands (for M = La, Ce, Eu, U, Pu, Am, Cm) to probe the effects of N-donation on the electronic structures and hence our previous conclusions.

Computational Details

A. General Procedures. All calculations were carried out using gradient-corrected density functional theory (DFT), as implemented in the *Gaussian* (G03)[16] and *Amsterdam Density Functional* (ADF)[17−21] quantum chemical codes. Spin-unrestricted calculations were performed on all Ln and An complexes to account for the formal f^n configurations of each Ln^{III} and An^{III} ion with the exception of the formally La^{III} f^0 ion, on which spin-restricted calculations were performed. As with our previous study,[7,8] all calculations were carried out within the D_3 point group.

B. *Gaussian 03*. The generalized gradient approximation functional Perdew−Burke−Ernzerhof (PBE)[22,23] was used for all G03 calculations. (14s 13p 10d 8f)/[10s 9p 5d 4f] segmented valence basis sets with Stuttgart−Bonn variety relativistic effective core potentials (RECPs) were used for the actinides,[24] and a (14s 13p 10d 8f)/[10s 8p 5d 4f] segmented valence basis set with a Stuttgart−Bonn RECP was used for each lanthanide.[25] 6-31G* basis sets were used for the O, S, Se, N, C, and P atoms, and the smaller 6-31G set was used for the H atom. Te was described with a (4s 5p)/[2s 3p] Stuttgart basis set[26] augmented to (4s 5p 7d)/[2s 3p 3d] with STO-3G*[27,28] polarization functions (for consistency because 6-31G* includes polarization functions on O, S, and Se); a Stuttgart RECP was also used for Te.[26] We have previously checked the validity of this Te basis set.[7,8]

For six-coordinate $M[N(EPH_2)_2]_3$ (models for the experimental ^{i}Pr compounds), the default values for the integration grid ("fine") and the convergence criteria (max force = 4.5×10^{-4} au Å^{-1}; SCF = 10^{-8}) were used for all optimizations bar those of Pr and Pu. For these compounds, the following convergence criteria were achieved: $Pr[N(SPH_2)_2]_3$ (max force = 8×10^{-4} au Å^{-1}; SCF = 10^{-7}), $Pr[N(SePH_2)_2]_3$ (max force = 8.5×10^{-4} au Å^{-1}; SCF = 10^{-6}), $Pr[N(TePH_2)_2]_3$ (max force = 1×10^{-3} au Å^{-1}; SCF = 10^{-5}), $Pu[N(OPH_2)_2]_3$ (max force = 7×10^{-4} au Å^{-1}; SCF = 10^{-7}),

(16) Frisch, M. J.; Trucks, G. W.; Schlegel, H. B.; Scuseria, G. E.; Robb, M. A.; Cheeseman, J. R.; Montgomery, J. J. A.; Vreven, T.; Kudin, K. N.; Burant, J. C.; Millam, J. M.; Iyengar, S. S.; Tomasi, J.; Barone, V.; Mennucci, B.; Cossi, M.; Scalmani, G.; Rega, N.; Petersson, G. A.; Nakatsuji, H.; Hada, M.; Ehara, M.; Toyota, K.; Fukuda, R.; Hasegawa, J.; Ishida, M.; Nakajima, T.; Honda, Y.; Kitao, O.; Nakai, H.; Klene, M.; Li, X.; Knox, J. E.; Hratchian, H. P.; Cross, J. B.; Adamo, C.; Jaramillo, J.; Gomperts, R.; Stratmann, R. E.; Yazyev, O.; Austin, A. J. ; Cammi, R.; Pomelli, C.; Ochterski,J. W. ; Ayala, P. Y.; Morokuma, K.; Voth, G. A. ; Salvador, P.; Dannenberg, J. J.; Zakrzewski, V. G.; Dapprich, S.; Daniels, A. D.; Strain, M. C.; Farkas, O.; Malick, D. K.; Rabuck, A. D.; Raghavachari, K.; Foresman, J. B.; Ortiz, J. V.; Cui, Q.; Baboul, A. G.; Clifford, S.; Cioslowski, J.; Stefanov, B. B.; Liu, G.; Liashenko, A.; Piskorz, P.; Komaromi, I.; Martin, R. L.; Fox, D. J.; Keith, T.; Al-Laham, M. A.; Peng, C. Y.; Nanayakkara, A.; Challacombe, M.; Gill, P. M. W.; Johnson, B.; Chen, W.; Wong, M. W.; Gonzalez, C.; Pople, J. A. *Gaussian*; Gaussian Inc.: Pittsburgh, PA, 2003.

(17) *ADF 2006*; Department of Theoretical Chemistry, Vrije Universiteit: Amsterdam, The Netherlands, 2006.

(18) Baerends, E. J.; Ellis, D. E.; Ros, P. *Chem. Phys.* **1973**, *2*, 41.

(19) Versluis, L.; Ziegler, T. *J. Chem. Phys.* **1988**, *88*, 322.

(20) te Velde, G.; Baerends, E. J. *J. Comput. Phys.* **1992**, *99*, 84.

(21) Fonseca Guerra, C.; Snijders, J. G.; te Velde, G.; Baerends, E. J. *Theor. Chem. Acc.* **1998**, *99*, 391.

(22) Perdew, J. P.; Burke, K.; Ernzerhof, M. *Phys. Rev. Lett.* **1996**, *77*, 3865.

(23) Perdew, J. P.; Burke, K.; Ernzerhof, M. *Phys. Rev. Lett.* **1997**, *78*, 1396.

(24) Cao, X. Y.; Dolg, M. *THEOCHEM* **2004**, *673*, 203.

(25) Cao, X. Y.; Dolg, M. *THEOCHEM* **2002**, *581*, 139.

(26) Bergner, A.; Dolg, M.; Kuechle, W.; Stoll, H.; Preuss, H. *Mol. Phys.* **1993**, *80*, 1431.

(27) Collins, J. B.; Schleyer, P. V. R.; Binkley, J. S.; Pople, J. A. *J. Chem. Phys.* **1976**, *64*, 5142.

(28) Hehre, W. J.; Stewart, R. F.; Pople, J. A. *J. Chem. Phys.* **1969**, *59*, 2657.

Table 1. Experimental and Calculated r(Ln−E)/Å in Ln[N(EPH$_2$)$_2$]$_3$ and Ln[N(EPPh$_2$)$_2$]$_3$

	Ln[N(OPH$_2$)$_2$]$_3$[a]	Ln[N(SPH$_2$)$_2$]$_3$[a]		Ln[N(SPPh$_2$)$_2$]$_3$		Ln[N(SePH$_2$)$_2$]$_3$[a]		Ln[N(SePPh$_2$)$_2$]$_3$		Ln[N(TePH$_2$)$_2$]$_3$[a]	
	calcd Ln−O	exptl Ln−S	calcd Ln−S	exptl Ln−S	calcd Ln−S	exptl Ln−Se	calcd Ln−Se	exptl Ln−Se	calcd Ln−Se	exptl Ln−Te	calcd Ln−Te
La	2.417	2.892	2.916	3.021	3.070	3.019	3.027	3.123	3.153	3.224	3.232
Ce	2.390	2.864	2.890	3.005	3.046		2.996	3.101	3.128	3.182	3.202
Pr	2.373		2.870				2.979				3.187
Pm	2.348		2.851				2.961				3.173
Eu	2.335		2.873		3.003		2.985		3.127		3.20

[a] Data from ref 8 (experimental data for Ln[N(EP^{i}Pr)$_2$]$_3$).

Pu[N(SPH$_2$)$_2$]$_3$ (max force = 8 × 10^{-4} au Å^{-1}; SCF = 10^{-5}), Pu[N(SePH$_2$)$_2$]$_3$ (max force = 5 × 10^{-4} au Å^{-1}; SCF = 10^{-8}), and Pu[N(TePH$_2$)$_2$]$_3$ (max force = 8 × 10^{-4} au Å^{-1}; SCF = 10^{-5}). For nine-coordinate M[N(EPPh$_2$)$_2$]$_3$ (E = S, Se), the default values for the integration grid and convergence criteria were used for all La, Ce, and U geometry optimizations. The Eu, Pu, and Am calculations were more problematic, and the following convergence criteria were achieved: Eu[N(EPPh$_2$)$_2$]$_3$ (E = S, Se; max force = 3 × 10^{-3} au Å^{-1}; SCF = 10^{-8}), Pu[N(SPPh$_2$)$_2$]$_3$ (max force = 4.5 × 10^{-4} au Å^{-1}; SCF = 10^{-5}), [Pu(N(SePPh$_2$)$_2$)$_3$] (max force = 5 × 10^{-4} au Å^{-1}; SCF = 10^{-5}), and Am[N(EPPh$_2$)$_2$]$_3$ (E = S, Se; max force = 3 × 10^{-3} au Å^{-1}; SCF = 10^{-8}).

As with our previous studies of M[N(EH$_2$)$_2$]$_3$,[7,8] little spin contamination was found in any of the open-shell six-coordinate complexes, with the values of $\langle S^2 \rangle$ being extremely close to the ideal values in all cases. This is also the case for nine-coordinate M[N(EPh$_2$)$_2$]$_3$, with 12.05 being the largest deviation from the ideal value of 12.0 for Eu[N(SPh$_2$)$_2$]$_3$.

Natural charge and population analyses[29,30] were carried out in single-point calculations performed on the six-coordinate [M(N(EH$_2$)$_2$)$_3$] complexes and also on structures derived from the optimized nine-coordinate [M(N(EPh$_2$)$_2$)$_3$] structures, in which the Ph groups were replaced with H atoms. We have used the default partitioning scheme, in which the actinide 6d orbitals are placed in the Rydberg basis. While there is evidence that the 6d orbitals may be more appropriately considered as valence in the NPA scheme,[35] we have no direct experience with such a partitioning and have decided to retain the default approach so as to facilitate a direct comparison with our previous study.

C. ADF. PBE single-point calculations on optimized G03 structures were carried out in ADF. As above, for all M[N(EPPh$_2$)$_2$]$_3$ structures, the Ph groups were replaced in these single points by H atoms. TZP zero-order regular approximation (ZORA) basis sets were used for each of the f elements together with DZP ZORA basis sets for all other atoms bar H, for which DZ was used, and Te. ADF does not have a DZP basis set for Te, and so TZP polarization functions were added to the DZ basis. The frozen-core approximation was used. A 5d core was used for each actinide, 4d for the lanthanides and Te, 3d for Se, 2p for S and P, and 1s for O and N. Mulliken overlap population analyses[31,32] were carried out.

Results and Discussion

A. Geometries. In our previous study of six-coordinate M[N(EP^{i}Pr$_2$)$_2$]$_3$, we found that replacing the ^{i}Pr groups with H atoms (or CH$_3$ groups) had a minimal effect upon the optimized metal−ligand bond lengths.[7,8] Furthermore, we were able to obtain optimized geometries for all six-coordinate species studied; i.e., it was possible to converge structures with E = O-, S-, Se-, and Te-donor ligands for La, Ce, U, and Pu. This also proved to be the case in the present extension of these calculations to Pr, Pm, Eu, Np, Am, and Cm.

When moving to nine-coordinate M[N(EPPh$_2$)$_2$]$_3$, we began by replacing the Ph groups with H atoms. Unfortunately, the agreement between theory and experiment for the La, Ce, U, and Pu systems with E = S and Se was not satisfactory, and so we reoptimized including the full ligands. Agreement with the experiment was much improved, although the best agreement was obtained only when the P−N−P bond angle was constrained in the calculations to the experimentally observed angle (ca. 147° for the S complexes and 144° for the Se). In subsequent calculations on the Eu, Am, and Cm complexes, we therefore constrained this angle to be 147° in the S systems and 144° in the Se. The maximum energy difference between structures obtained with and without constrained P−N−P angles was 9.8 kJ/mol (for U[N(SePPh$_2$)$_2$]$_3$). Subsequently, the phenyl groups were replaced by H atoms in single-point calculations so as to facilitate a comparison with the H models for six-coordinate M[N(EP^{i}Pr$_2$)$_2$]$_3$.

It proved impossible to obtain nine-coordinate M[N(EPPh$_2$)$_2$]$_3$ structures for O- and Te-donor ligands. In all cases with these ligands, the final structures were six-coordinate, with the N atoms moving away from their starting positions around the metal center to nonbonding distances. These structures will not be discussed further.

The calculated metal−chalcogen distances for six-coordinate M[N(EPH$_2$)$_2$]$_3$ and nine-coordinate M[N(EPPh$_2$)$_2$]$_3$ are given in Tables 1 (Ln) and 2 (An), together with the experimental data for M[N(EP^{i}Pr$_2$)$_2$]$_3$ and M[N(EPPh$_2$)$_2$]$_3$. The experimental and some of the calculated data are taken from ref 8 and are reproduced here to facilitate a comparison across the full range of systems studied. Comparison of experimental and calculated data for r(M−E) for six-coordinate M[N(EPH$_2$)$_2$]$_3$ (M = La, Ce, U, Pu) has been previously discussed[8] and will not be repeated here. Extension of our lanthanide study to Pr, Pm, and Eu reveals a steady decrease in r(M−O), by contrast to the compounds of the heavier chalcogens, for which a decrease to Pm is followed by an increase to Eu. The increase from Pm to Eu is 0.022 Å for E = S, rising to 0.024 Å for Se and 0.032 Å for Te. The difference between O and Te is clearly illustrated

(29) Carpenter, J. E.; Weinhold, F. *THEOCHEM* **1988**, *169*, 41.
(30) Weinhold, F.; Carpenter, J. E. *The Structure of Small Molecules and Ions*, Naaman, R., Vager, Z., Eds.; Plenum Press: New York, 1988; pp 227–236.
(31) Mulliken, R. S. *J. Chem. Phys.* **1955**, *23*, 1833, 1841, 2338, and 2343.
(32) Mulliken, R. S. *J. Am. Chem. Soc.* **1955**, *77*, 884.
(33) Denecke, M. A.; Rossberg, A.; Panak, P. J.; Weigl, M.; Schimmelpfennig, B.; Geist, A. *Inorg. Chem.* **2005**, *44*, 8418.

Table 2. Experimental and Calculated *r*(An−E)/Å in An[N(EPH$_2$)$_2$]$_3$ and An[N(EPPh$_2$)$_2$]$_3$

	An[N(OPH$_2$)$_2$]$_3$[a]	An[N(SPH$_2$)$_2$]$_3$[a]		An[N(SPPh$_2$)$_2$]$_3$		An[N(SePH$_2$)$_2$]$_3$[a]		An[N(SePPh$_2$)$_2$]$_3$		An[N(TePH$_2$)$_2$]$_3$[a]	
	calcd An−O	exptl An−S	calcd An−S	exptl An−S	calcd An−S	exptl An−Se	calcd An−Se	exptl An−Se	calcd An−Se	exptl An−Te	calcd An−Te
U	2.393	2.854	2.849	2.996	3.005	2.964	2.955	3.087	3.062	3.64	3.126
Np	2.381		2.840				2.931				3.132
Pu	2.364	2.819	2.830	2.978	3.003	2.917	2.932	3.071	3.075	3.123	3.135
Am	2.358		2.835		3.011		2.940		3.089		3.149
Cm	2.355		2.826		3.010		2.931		3.079		3.13

[a] Data from ref 8 (experimental data for An[N(EP^{i}Pr)$_2$]$_3$).

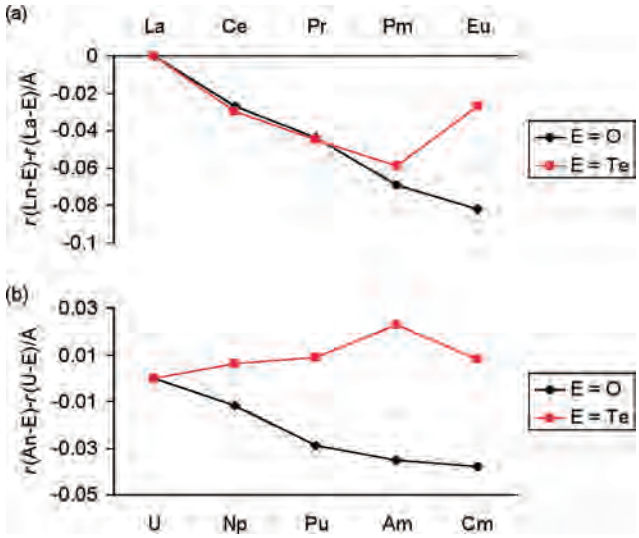

Figure 1. Normalized variation in *r*(M−E) in six-coordinate M[N(OPH$_2$)$_2$]$_3$ and M[N(TePH$_2$)$_2$]$_3$ for (a) M = Ln and (b) M = An.

Table 3. Experimental and Calculated *r*(Ln−N)/Å in Ln[N(EPPh$_2$)$_2$]$_3$

	Ln[N(SPPh$_2$)$_2$]$_3$		Ln[N(SePPh$_2$)$_2$]$_3$	
	exptl[a]	calcd	exptl[a]	calcd
La	2.652	2.706	2.706	2.762
Ce	2.637	2.687	2.691	2.747
Pr				
Pm				
Eu		2.690		2.761

[a] Data from ref 8.

in Figure 1, which plots the variation in *r*(M−E) in six-coordinate M[N(OPH$_2$)$_2$]$_3$ and M[N(TePH$_2$)$_2$]$_3$ for Ln and An, normalized to the values for La and U, respectively. As with the lanthanides, *r*(An−E) for An[N(OPH$_2$)$_2$]$_3$ decreases from M = U to Cm, although not as much as that from La to Eu. However, *r*(An−S) behaves differently, with a decrease from U to Pu, followed by an increase to Am and then another reduction at Cm. The increase from Pu to Am is also evident in the Se and Te compounds. Indeed, the trend in *r*(An−Te) is very different from that of the O systems, with the shortest value being at U and the largest at Am (Figure 1b). We previously attributed the short U−Te distance to enhanced covalency.[8] We note the seemingly anomalously long *r*(Eu−E) and *r*(Am−E) (E = S, Se, Te) and will return to this later.

Tables 3 (Ln) and 4 (An) present calculated *r*(M−N) for M[N(SPPh$_2$)$_2$]$_3$ and M[N(SePPh$_2$)$_2$]$_3$, with the experimental data being taken from ref 8. In all cases, the calculation slightly overestimates *r*(M−N), with the poorest agreement with the experiment being for Pu[N(SePPh$_2$)$_2$]$_3$ (0.074 Å).

Table 4. Experimental and Calculated *r*(An−N)/Å in An[N(EPPh$_2$)$_2$]$_3$

	An[N(SPPh$_2$)$_2$]$_3$		An[N(SePPh$_2$)$_2$]$_3$	
	exptl[a]	calcd	exptl[a]	calcd
U	2.632	2.674	2.701	2.726
Np				
Pu	2.612	2.675	2.668	2.742
Am		2.669		2.742
Cm		2.652		2.719

[a] Data from ref 8.

Table 5. Natural Charges for Ln[N(EPH$_2$)$_2$]$_3$ (as Models for the ^{i}Pr Compounds) and Ln[N(EPH$_2$)$_2$]$_3$//Ln[N(EPPh$_2$)$_2$]$_3$ (as Models for the Ph Compounds)

	Ln[N(EPH$_2$)$_2$]$_3$(^{i}Pr)[a]				Ln[N(EPH$_2$)$_2$]$_3$(Ph)	
	O	S	Se	Te	S	Se
La	2.49	2.12	2.03	1.83	2.18	2.12
E_{La}	−1.17	−0.73	−0.65	−0.49	−0.64	−0.57
P_{La}	1.60	1.02	0.93	0.78	1.08	0.99
N_{La}	−1.42	−1.33	−1.31	−1.29	−1.55	−1.53
$\Delta(q_{nat,La} - q_{nat,E_{La}})$	3.66	2.85	2.68	2.33	2.82	2.69
Ce	2.43	2.04	1.95	1.77	2.11	2.06
E_{Ce}	−1.17	−0.72	−0.64	−0.48	−0.64	−0.57
P_{Ce}	1.60	1.02	0.93	0.78	1.01	0.99
N_{Ce}	−1.42	−1.33	−1.31	−1.29	−1.54	−1.52
$\Delta(q_{nat,Ce} - q_{nat,E_{Ce}})$	3.60	2.76	2.59	2.25	2.75	2.63
Pr	2.42	2.03	1.93	1.74		
E_{Pr}	−1.16	−0.71	−0.63	−0.48		
P_{Pr}	1.59	1.01	0.93	0.78		
N_{Pr}	−1.42	−1.33	−1.31	−1.29		
$\Delta(q_{nat,Pr} - q_{nat,E_{Pr}})$	3.58	2.74	2.56	2.22		
Pm	2.46	2.01	1.90	1.71		
E_{Pm}	−1.17	−0.71	−0.63	−0.47		
P_{Pm}	1.59	1.02	0.93	0.77		
N_{Pm}	−1.42	−1.33	−1.31	−1.29		
$\Delta(q_{nat,Pm} - q_{nat,E_{Pm}})$	3.62	2.72	2.53	2.18		
Eu	2.41	1.88	1.79	1.60	1.97	1.89
E_{Eu}	−1.16	−0.69	−0.61	−0.45	−0.64	−0.51
P_{Eu}	1.59	1.01	0.93	0.78	1.08	0.98
N_{Eu}	−1.42	−1.32	−1.31	−1.29	−1.53	−1.50
$\Delta(q_{nat,Eu} - q_{nat,E_{Eu}})$	3.57	2.58	2.39	2.06	2.61	2.40

[a] Data for the La and Ce compounds from ref 8.

B. Natural Charges and Populations. The natural charges for the metal atoms and the atoms in the ligand backbone are collected in Tables 5 (Ln) and 6 (An). It is noticeable that for all M, with the exception of U, the charge is higher in the nine-coordinate systems than in the analogous six-coordinate system. The nitrogen charge is consistently ca. 0.2 units larger in the former, and the chalcogen atoms have a smaller charge. The overall result is that the charge difference between the metal and chalcogen is very similar in the two families of compounds, for all of the Ln systems and the An compounds bar those of U and to a lesser extent Am, suggesting that moving to the nine-coordinate systems does not significantly perturb the ionicity of the metal−chalcogen bond.

Table 6. Natural Charges for An[N(EPH$_2$)$_2$]$_3$ (as Models for the ^{i}Pr Compounds) and An[N(EPH$_2$)$_2$]$_3$//An[N(EPPh$_2$)$_2$]$_3$ (as Models for the Ph Compounds)

	An[N(EPH$_2$)$_2$]$_3$(^{i}Pr)[a]				An[N(EPH$_2$)$_2$]$_3$(Ph)	
	O	S	Se	Te	S	Se
U	2.21	1.70	1.62	1.52	1.59	1.53
E_U	−1.13	−0.67	−0.60	−0.44	−0.58	−0.51
P_U	1.59	1.02	0.93	0.78	1.09	1.00
N_U	−1.42	−1.32	−1.31	−1.29	−1.50	−1.48
$\Delta(q_{nat,U} - q_{nat,E_U})$	3.35	2.37	2.22	1.97	2.17	2.04
Np	2.24	1.82	1.73	1.61		
E_{Np}	−1.14	−0.69	−0.60	−0.46		
P_{Np}	1.60	1.02	0.93	0.78		
N_{Np}	−1.42	−1.33	−1.31	−1.29		
$\Delta(q_{nat,Np} - q_{nat,E_{Np}})$	3.38	2.51	2.34	2.07		
Pu	2.29	1.87	1.78	1.61	1.89	1.85
E_{Pu}	−1.14	−0.70	−0.61	−0.46	−0.62	−0.54
P_{Pu}	1.60	1.02	0.93	0.78	1.09	1.00
N_{Pu}	−1.42	−1.32	−1.31	−1.29	−1.52	−1.50
$\Delta(q_{nat,Pu} - q_{nat,E_{Pu}})$	3.43	2.57	2.39	2.07	2.51	2.39
Am	2.37	1.87	1.79	1.58	2.06	1.96
E_{Am}	−1.16	−0.69	−0.61	−0.45	−0.62	−0.55
P_{Am}	1.59	1.02	0.93	0.78	1.08	0.99
N_{Am}	−1.42	−1.32	−1.31	−1.29	−1.53	−1.51
$\Delta(q_{nat,Am} - q_{nat,E_{Am}})$	3.53	2.56	2.40	2.03	2.68	2.51
Cm	2.50	2.08	1.99	1.80	2.16	2.10
E_{Cm}	−1.18	−0.78	−0.65	−0.49	−0.65	−0.58
P_{Cm}	1.60	1.02	0.93	0.78	1.08	0.99
N_{Cm}	−1.42	−1.33	−1.31	−1.29	−1.54	−1.51
$\Delta(q_{nat,Cm} - q_{nat,E_{Cm}})$	3.68	2.81	2.63	2.29	2.81	2.68

[a] Data for the U and Pu compounds from ref 8.

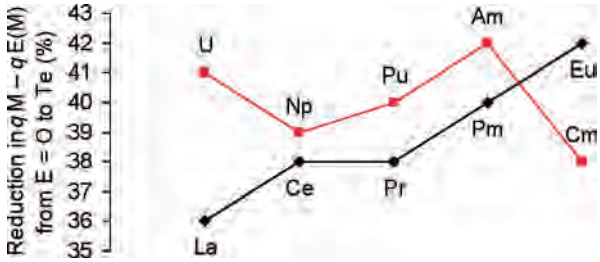

Figure 2. Percent reduction in $q_M - q_{E(M)}$ from E = O to Te in six-coordinate M[N(EPH$_2$)$_2$]$_3$.

In our previous study of La, Ce, U, and Pu systems, we examined the charge differences between M and E as a function of both metal and chalcogen.[8] The reduction in $q_M - q_{E_M}$ as E is altered from O to Te was smallest for La and most for U; i.e., the decrease in the ionicity down group 16 is largest for the U compounds and smallest for the La compounds. Figure 2 shows this reduction for all of our six-coordinate M[N(EPH$_2$)$_2$]$_3$. In general, the values for the lanthanide systems are smaller than those for the actinides, suggesting that the lanthanides are more ionic. There is a general upward trend in the Ln values and a significantly greater reduction in the ionicity down group 16 for Eu than for La (42% vs 36%). The value for Am is the same as that for Eu, while Cm is much reduced from Am, with the smallest value of any actinide 38%, comparable to the early lanthanides.

The natural atomic orbital populations for the metals are presented in Tables 7 and 8. The values given have been obtained by subtracting the formal values from the calculated ones; i.e., they show the enhancement of the populations above the formal. In each case, the latter is 2 for the s orbitals, 6 for the p, and 0 for the d. The formal f populations vary

Table 7. Natural Populations for Ln[N(EPH$_2$)$_2$]$_3$ (as a Model for the ^{i}Pr Compounds) and Ln[N(EPH$_2$)$_2$]$_3$//Ln[N(EPPh$_2$)$_2$]$_3$ (as a Model for the Ph Compounds)

	Ln[N(EPH$_2$)$_2$]$_3$(^{i}Pr)[a]				Ln[N(EPH$_2$)$_2$]$_3$(Ph)	
	O	S	Se	Te	S	Se
			La Compounds			
s	0.12	0.28	0.34	0.42	0.26	0.30
p	0.01	0.01	0.01	0.02	0.01	0.01
d	0.19	0.41	0.46	0.57	0.30	0.33
f(0)	0.23	0.20	0.18	0.16	0.22	0.22
			Ce Compounds			
s	0.13	0.29	0.35	0.43	0.28	0.31
p	0.01	0.01	0.01	0.02	0.01	0.01
d	0.19	0.40	0.46	0.56	0.33	0.34
f(1)	0.27	0.27	0.24	0.22	0.27	0.28
			Pr Compounds			
s	0.14	0.30	0.36	0.44		
p	0.01	0.01	0.01	0.02		
d	0.19	0.40	0.44	0.53		
f(2)	0.27	0.28	0.27	0.28		
			Pm Compounds			
s	0.15	0.31	0.37	0.45		
p	0.01	0.01	0.01	0.02		
d	0.18	0.37	0.40	0.47		
f(4)	0.23	0.31	0.33	0.35		
			Eu Compounds			
s	0.16	0.32	0.38	0.44	0.29	0.32
p	0.01	0.01	0.01	0.02	0.01	0.02
d	0.17	0.27	0.30	0.35	0.22	0.23
f(6)	0.27	0.52	0.53	0.59	0.52	0.54

[a] Data for the La and Ce compounds from ref 8. All values are given as the "excess" over and above the formal values 2 for s, 6 for p, and 0 for d and given in parentheses in the table for the f.

and are shown in parentheses in the tables. Turning to the six-coordinate data, it is apparent that the $(n - 1)$p populations are essentially unaltered from their formal value in all cases. By contrast, there are increases of the other orbital populations above their formal values, which is typically taken as evidence of the involvement of these orbitals in covalent bonding with the ligands. For all metals, the s population increases as group 16 is descended, and the extent of this increase is broadly similar for all metals, with slightly larger values for the An complexes than the Ln. The d populations also increase down group 16, by an amount that is generally slightly more significant than that for the s. This increase is rather similar for all metals, with the exception of Eu and U, for which it is smaller and larger respectively than for the other metals. For the nine-coordinate systems, the s and d populations are slightly smaller than those in the analogous six-coordinate complexes.

Figure 3 shows the enhanced f populations for all of the six-coordinate complexes. In our previous study, we noted that, by contrast to the d and the s populations, there was no significant increase in the f population from O to Te in the La, Ce, U, and Pu systems and that the f populations were larger for U and Pu. We concluded that increases in the covalency down group 16 are a function of the metal s and d orbitals and that the actinide complexes are more covalent than their lanthanide counterparts on account of the greater involvement of the 5f orbitals over the 4f orbitals. Figure 3 suggests that the latter conclusion becomes increasingly less valid on moving to the right in the 4f and 5f series and must

Table 8. Natural Populations for $An[N(EPH_2)_2]_3$ (as a Model for the ^iPr Compounds) and $An[N(EPH_2)_2]_3$//$An[N(EPPh_2)_2]_3$ (as a Model for the Ph Compounds)[a]

	$An[N(EPH_2)_2]_3$ (^iPr) [a]				$An[N(EPH_2)_2]_3$ (Ph)	
	O	S	Se	Te	S	Se
			U Compounds			
s	0.16	0.36	0.43	0.51	0.31	0.36
p	0.01	0.01	0.01	0.01	0.02	0.02
d	0.17	0.35	0.43	0.62	0.28	0.31
f(3)	0.33	0.47	0.38	0.29	0.52	0.54
			Np Compounds			
s	0.17	0.37	0.43	0.50		
p	0.02	0.01	0.01	0.01		
d	0.17	0.34	0.43	0.54		
f(4)	0.38	0.40	0.36	0.31		
			Pu Compounds			
s	0.17	0.37	0.44	0.50	0.32	0.36
p	0.01	0.01	0.01	0.02	0.02	0.02
d	0.17	0.34	0.38	0.48	0.27	0.28
f(5)	0.35	0.38	0.37	0.36	0.44	0.45
			Am Compounds			
s	0.18	0.38	0.44	0.51	0.33	0.36
p	0.01	0.01	0.01	0.01	0.02	0.02
d	0.16	0.29	0.34	0.41	0.26	0.27
f(6)	0.27	0.44	0.41	0.47	0.32	0.37
			Cm Compounds			
s	0.19	0.39	0.45	0.52	0.34	0.38
p	0.01	0.01	0.01	0.02	0.02	0.02
d	0.17	0.34	0.39	0.49	0.28	0.30
f(7)	0.13	0.15	0.14	0.15	0.17	0.18

[a] Data for the U and Pu compounds from ref 8. All values are given as the "excess" over and above the formal values 2 for s, 6 for p, and 0 for d and given in parentheses in the table for the f.

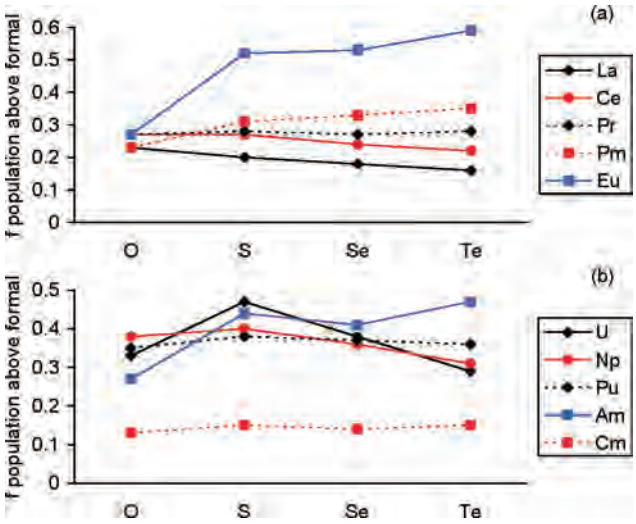

Figure 3. Natural f population above the formal value in six-coordinate $M[N(EPH_2)_2]_3$ for (a) M = Ln and (b) M = An.

be reassessed for Eu, Am, and Cm. In the lanthanides, Pr and Pm are not very different from La and Ce. Eu, however, is quite different, with much enhanced f populations in its complexes with S-, Se-, and Te-based ligands. By contrast, Cm has f populations that are much reduced from those of U, Np, and Pu, below even the La values. Am, however, which might be expected to display behavior intermediate between that of Pu and Cm, has the largest f population of all of the actinide Se and Te complexes and has a trend down group 16 that is more reminiscent of Eu than any other metal. We will return to the origins and implications of the f populations in Eu, Am, and Cm in section D.

In the nine-coordinate lanthanide complexes, the enhanced f populations are generally slightly larger than those in analogous six-coordinate systems, and the significantly enhanced f populations for Eu seen in the latter are also found in the former. The nine-coordinate actinide complexes also display slightly enhanced f populations over their six-coordinate analogues, with the exception of the Am systems, which display behavior closer to what might be anticipated; i.e., they follow the gradual reduction in enhanced f population as the series is crossed. We do not know why the f populations in the nine-coordinate Am complexes are less than those in their six-coordinate counterparts. The differences are small (0.12 electrons in the S complexes and only 0.04 electrons in the Se complexes) but not negligible.

C. Molecular Orbital (MO) Analysis. In order to test further the conclusions drawn from the natural and Mulliken analyses, we have probed the MO structure of the target complexes. MO energy level diagrams for six-coordinate $M[N(EPH_2)_2]_3$ (E = O, S, Se, Te) are given in Figure 4 for M = La, Ce, Pr, Pm, and Eu and Figure 5 for M = U, Np, Pu, Am, and Ce. The La and U diagrams are taken from our previous study[8] and are included here to facilitate comparison with the complexes of the other metals. In order to allow the electronic structures to be better compared, Figures 4a and 5a have been constructed by arbitrarily setting the energy of the lowest unoccupied orbital of each of the La complexes to an energy of 0 eV. This orbital (number 53) is predominantly (more than 95%) 4f in character in all four cases. For the other Ln and An systems, the highest occupied orbitals contain the anticipated f electrons, and the energy of the most stable of these orbitals has been set to 0 eV in all cases. Given the open-shell nature of all of the complexes bar those of La, spin-unrestricted calculations were performed, yielding separate energies for the α- and β-spin components of each spatial orbital. Figures 4 and 5 present the mean energies of the α- and β-spin components of each spatial MO.

As we noted previously,[8] in $La[N(EPH_2)_2]_3$ (E = O, S, Se, Te) orbital 53 (the LUMO) is well separated from the highest occupied levels by an energy gap that decreases from just over 5 eV in $La[N(OPH_2)_2]_3$ to just under 3 eV in $La[N(TePH_2)_2]_3$. Below the highest occupied MO (orbital 52), there is a group of 18 orbitals that spans a 2−3 eV energy range and that is well separated from the next group of orbitals below (represented by the open-ended black boxes in Figure 4a). The 18 orbitals from 35 to 52 are predominantly chalcogen *n*p-based in all cases. It is clear that their barycenter moves relative to the La 4f-based orbitals as group 16 is descended; this is a result of the *n*p atomic orbital energies becoming less negative as the chalcogen becomes heavier.

Parts b−e of Figure 4 reveal that, in general, the valence electronic structures of the other lanthanide complexes are rather similar to those of the La systems, with the one significant difference being that, as the lanthanide series is crossed, the 4f-based manifold becomes closer in energy to the ligand levels. Indeed, for the Eu complexes with the heavier chalcogens, the highest occupied orbitals are no

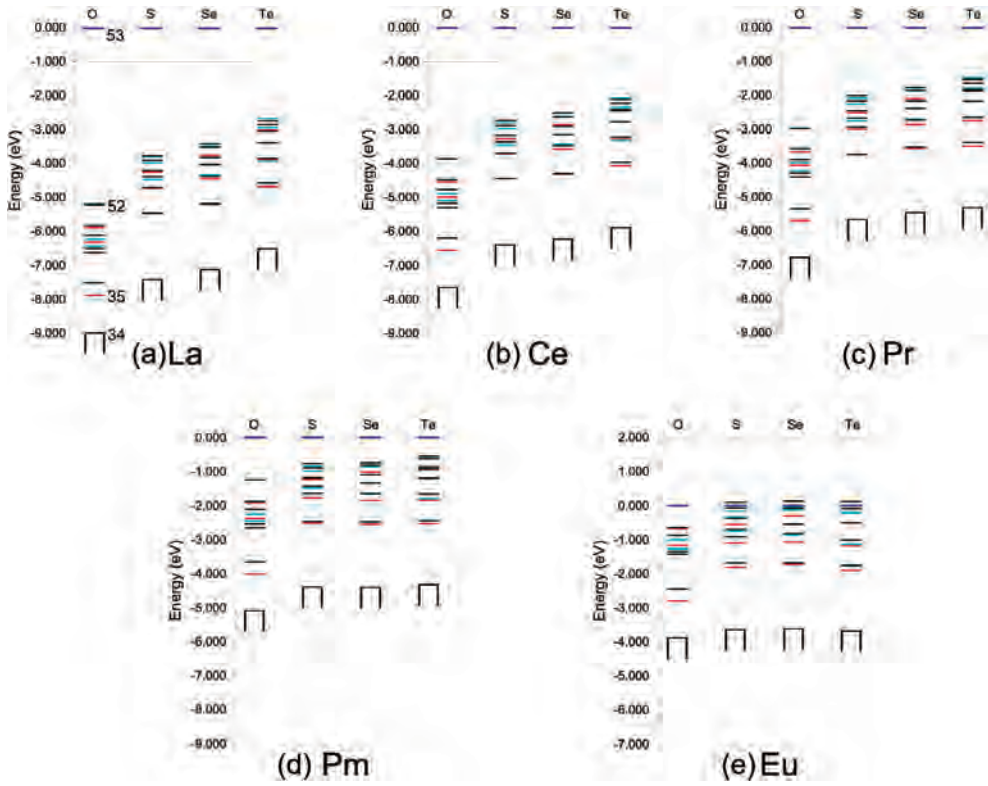

Figure 4. MO energy level diagrams for $Ln[N(EPH_2)_2]_3$ (Ln = La, Ce, Pr, Pm, Eu; E = O, S, Se, Te). The energy of the lowest unoccupied orbital of each of the La complexes (number 53, shown in dark blue) has been set to an energy of 0 eV, as has the energy of the most stable of the highest occupied (4f-based) orbitals of the other Ln complexes (also shown in dark blue). The mean energies of the α- and β-spin components of each spatial MO are presented for the Ce, Pr, Pm, and Eu compounds. For orbitals 35−52, red indicates a_1 symmetry MOs, turquoise a_2 MOs, and black e MOs. Note the *y* axis scale change in part e.

longer 4f-based but are part of the chalcogen p-based group; the 4f levels now lie within the ligand manifold. Figure 5 reveals a similar pattern for the actinide systems, such that for the Cm complexes with the heavier chalcogens the 5f manifold is very much within the ligand levels.

Analysis of MO diagrams (not shown) for the nine-coordinate target systems reveals an electronic structure that is very similar to that of the analogous six-coordinate complexes. Similar energy gaps are found between the highest occupied ligand-based levels and the early 4f and 5f metal-based orbitals, and the trend across the series for the f-based levels to become increasingly isoenergetic with the ligand orbitals is also observed.

Our previous analysis of the metal content of the 18 chalcogen *n*p-based MOs of $M[N(EPH_2)_2]_3$ (M = La, U; E = O, S, Se, Te) suggested that the bulk of the covalent contribution to the metal−ligand bonding arises from metal d orbital character.[8] Examination (of orbital compositions and visual inspection of orbital pictures) of the present target systems revealed that the most extensive covalency is in an e pair of levels in the S complexes (orbitals 39 and 40). The percent metal d character of these orbitals is given for all 10 target complexes in Table 9, from which it can be seen that the contributions are all rather similar, with the exception of U and to a lesser extent Np, which have slightly larger d character than the other An compounds and all of the Ln compounds. Three-dimensional representations of orbitals 39 and 40 in 6 coordinate $Am[N(SPH_2)_2]_3$ are given in Figure 6, in which the metal d-based covalency can clearly be seen.

It is important to determine the extent of any f-based covalency. In our previous analysis of $M[N(EPH_2)_2]_3$ (M = La, U; E = O, S, Se, Te), we concluded that, while there was negligible La 4f covalency, there was a small but significant 5f covalency in the U systems, as averaged over the 18 chalcogen *n*p-based levels.[8] The MO diagrams presented in Figures 4 and 5 suggest that metal f orbital contributions to these orbitals might increase as the 4f and 5f series are crossed, as the energies of the metal and ligand levels come closer together. Given that Te is the softest of the chalcogen donors, we decided to examine the Te-based MOs for evidence of covalent interactions and, in particular, for those involving metal f orbitals. Somewhat different from the S complexes, the most significant metal contribution to the 18 Te-based orbitals is found in a less stable e pair, orbitals 45 and 46, and Table 10 contains the metal d and f contributions to these orbitals for the U, Np, Pu, and Am compounds. It is noticeable how the metal d content decreases as the 5f series is crossed, rather as found for MOs 39 and 40 of the S complexes. By contrast, the metal f contribution increases very significantly, such that it is much larger than the d contribution in $Am[N(TePH_2)_2]_3$. Does this mean that Am−Te covalency is dominated by the metal's 5f orbitals? Figure 7 suggests not. This figure presents a three-dimensional representation of orbital 45 of $Am[N(TePH_2)_2]_3$ (Figure 7a), together with, on the same scale, representations of the $5f_{xyz}$ (Figure 7b) and $6d_{xz}$ (Figure 7c) orbitals of Am, both of which contribute to orbital 45. The radial extension of the 6d orbital is much larger than that of

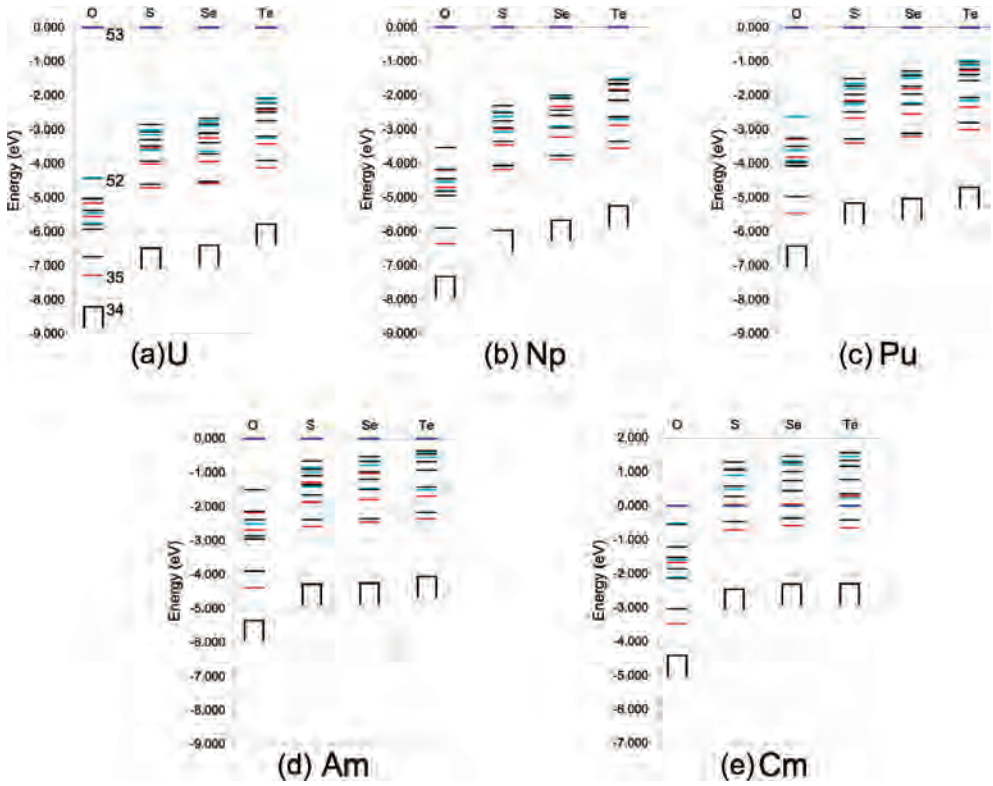

Figure 5. MO energy level diagrams for $An[N(EPH_2)_2]_3$ (An = U, Np, Pu, Am, Cm; E = O, S, Se, Te). The energy of the most stable of the highest occupied (5f-based) orbitals (number 53, shown in dark blue) has been set to an energy of 0 eV. The mean energies of the α- and β-spin components of each spatial MO are presented. For orbitals 35−52, red indicates a_1 symmetry MOs, turquoise a_2 MOs, and black e MOs. Note the *y* axis scale change in part e.

Table 9. Metal d Contribution (%) to MOs 39 and 40 of Six-Coordinate $M[N(SPH_2)_2]_3$

La	8.8	U	11.1
Ce	9.3	Np	10.2
Pr	8.4	Pu	8.8
Pm	7.5	Am	9.6
Eu	8.6	Cm	8.1

the 5f, and hence the covalency indicated in Figure 7a is highly unlikely to arise from the f orbitals. We suggest that the large Am f contribution to MOs 45 and 46 arises simply from the energetic proximity of the metal and ligand levels and does not imply significant f orbital covalency.

As noted above, in six-coordinate $Cm[N(TePH_2)_2]_3$, the highest occupied orbitals are not metal f-based. Rather, the f-based orbitals sit well down in the ligand manifold, such that analysis of the character of the MOs displayed in Figure 5e reveals some lower-lying orbitals with very high f content. A three-dimensional representation of orbital 39 of $Cm[N(TePH_2)_2]_3$ (a typical example) is shown in Figure 8. This is clearly a metal f-based orbital and has no significant ligand character at all. Indeed, analysis of the $Cm[N(TePH_2)_2]_3$ valence orbitals reveals that there are no levels with Cm 5f character that show Cm−Te covalency: the seven Cm f electrons sit energetically within the ligand manifold but do not mix with the Te 5p orbitals. Analysis of the equivalent MOs of $Eu[N(TePH_2)_2]_3$, which is similar to the Cm system in having the metal f-based MOs energetically proximate to the ligand levels, reveals a similar picture: there is very little evidence of 4f-based Eu−Te covalency.

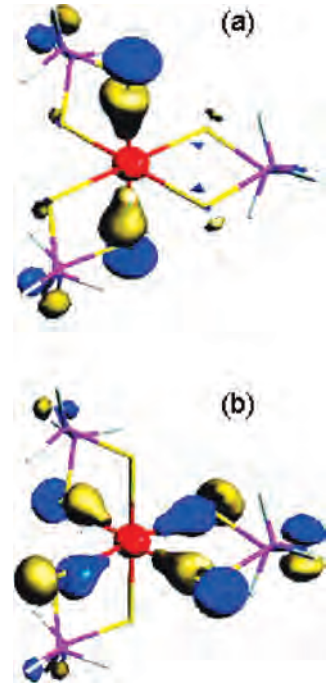

Figure 6. Three-dimensional representations of orbitals 39 and 40 in six-coordinate $Am[N(SPH_2)_2]_3$. The Molekel isosurface value is 0.375 in both cases.

D. Further Discussion of the Eu, Am, and Cm Complexes. Both the structural data and the natural charge and population analyses suggest that the six-coordinate Eu and Am complexes with the heavier chalcogens behave rather differently from what might be expected on the basis of the

Table 10. Metal d and f Contributions (%) to MOs 45 and 46 of Six-Coordinate $M[N(TePH_2)_2]_3$

	d	f
U	7.8	2.8
Np	6.9	4.0
Pu	6.0	6.0
Am	4.7	12.3

compounds of the other lanthanide and actinide metals studied. The Eu−E and Am−E bond lengths for the heavier chalcogens are longer than might be anticipated, the reduction in charge difference between M and E down group 16 is less, and the f populations are larger. These observations are generally supported by the nine-coordinate data. In our previous study, we took enhanced f populations in $U[N(EPH_2)_2]_3$ over analogous $La[N(EPH_2)_2]_3$ as evidence of greater metal−ligand covalency in the actinide systems. This was supported by analysis of the individual orbitals, in which U−E f-based covalency can be observed. However, as the actinide series is crossed, the 5f orbitals become radially more contracted and, as we have seen for six-coordinate $Am[N(TePH_2)_2]_3$, f orbital contribution to MOs does not necessarily translate to f-based covalency. Indeed, were the large f populations seen for $Eu[N(TePH_2)_2]_3$ and $Am[N(TePH_2)_2]_3$ evidence of f-based covalency, we might expect the Eu−Te and Am−Te bonds to be *shorter* than those in neighboring complexes, not longer, as is observed.

What, then, is the cause of the enhanced f populations in the Eu and Am systems? Eu^{III} and Am^{III} are formally f^6 ions. The allure of the half-filled shell may lead to Eu and Am centers that, for the heavier chalcogens at least, are closer to M^{II} than M^{III}; i.e., as the ligands become less electronegative down group 16, the metal centers move closer to f^7 (Eu in six-coordinate $Eu[N(TePH_2)_2]_3$ is $4f^{6.59}$, and Am in the analogous compound is $5f^{6.47}$). Given that the ionic radii of M^{II} are larger than those of M^{III}, the reduction of the positive charge on the metal centers leads to longer metal−chalcogen bonds. For the O compounds, the ligands are sufficiently electronegative so as to prevent this process from occurring, and both $Eu[N(OPH_2)_2]_3$ and $Am[N(OPH_2)_2]_3$ are not atypical in comparison with the other Ln−O and An−O complexes. Furthermore, it is noticeable how small the f populations are in the Cm complexes (Figure 3b); even $Cm[N(TePH_2)_2]_3$ is only $5f^{7.15}$. Cm^{III} is already formally $5f^7$ and is therefore reluctant to deviate significantly.

The partial charges calculated for Cm are in all cases the largest of any of the actinides with a given chalcogen (Table 6); the bonding in these complexes is very ionic in a formally $Cm^{3+}/[N(EPH_2)_2]_3^{3-}$ sense. By contrast, for Eu the charges are the smallest of any lanthanide for a given chalcogen (Table 5). However, this does not indicate appreciable covalency in the Eu−E bond but rather reflects a still ionic but more $Eu^{2+}/[N(EPH_2)_2]_3^{2-}$ picture in a formal sense. The latter description is probably also appropriate for Am with the heavier chalcogens; the charge on Am in $Am[N(TePH_2)_2]_3$ is less positive than that in all of the actinides bar U.

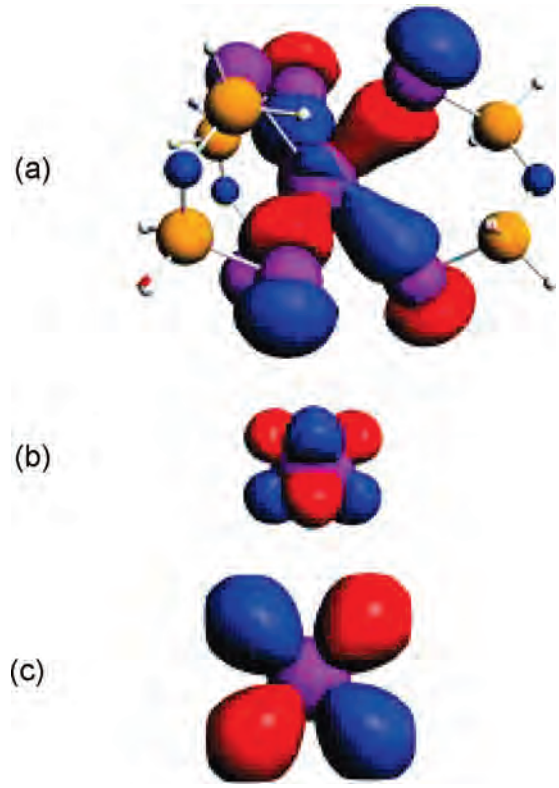

Figure 7. Three-dimensional representations of (a) orbital 45 in six-coordinate $Am[N(TePH_2)_2]_3$ and, on the same scale (ADFview isosurface value = 0.03), representations of the $5f_{xyz}$ (b) and $6d_{xz}$ (c) orbitals of Am, both of which contribute to orbital 45.

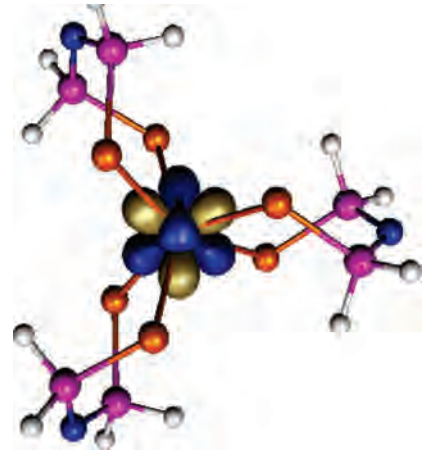

Figure 8. Three-dimensional representation of orbital 39 in six-coordinate $Cm[N(TePH_2)_2]_3$. The Molekel isosurface value is 0.4.

Conclusions

In this contribution, we have presented the results of DFT calculations on a series of six- and nine-coordinate complexes of the general formulas $Ln[N(EPH_2)_2]_3$ and $An[N(EPH_2)_2]_3$. Our aims were, for the six-coordinate systems, to extend our previous work on La, Ce, U, and Pu[7,8] to the right in both the 4f and 5f series and, for the nine-coordinate systems, to probe the effects of coordinating the metal not only by chalcogens atoms but also by the N atoms of the ligand backbone. The latter was found to make relatively little difference to the electronic structure and, in particular, to the metal−chalcogen interactions.

Extension to the middle of the f block, and in particular to Eu, Am, and Cm, has exposed some rather interesting features that might not have been anticipated. The longer than expected Eu−E and Am−E bond lengths, the smaller reduction in the charge difference between M and E down group 16, and the larger f populations all point to these metals having significant M^{II} character in their complexes with the heavier chalcogens, by contrast to Cm, which is very much Cm^{III} in all cases. This is possibly the result of the formal f^6 configuration of Eu^{III} and Am^{III}, one electron away from the half-filled shell.

We have looked hard for evidence of f orbital covalency as the 4f and 5f series are crossed. Although the largest f populations are found in the Eu and Am complexes of the heavier chalcogens, we do not equate this with f-based covalency; the radial extension of the f orbitals in the middle of the series is too small to permit significant metal−ligand overlap. Rather, any covalent interactions stem from the metal d orbitals and, to a lesser extent, the s orbitals. The localized nature of the f orbitals is best represented by the Cm systems, in which there is excellent energy match between the 5f electrons and the ligand levels but very little mixing in the resultant MOs.

It is already known that ligands based on moderately soft donors such as N and S selectively bind to the minor actinides with preference to Eu.[4,14,33,34] It is interesting to speculate as to whether, in principle at least, the very soft donor ligands studied here would also show selectivity for Am and Cm. We are, of course, unable to provide a complete answer to this question because the present study has focused primarily on bonding; we have not calculated metal−ligand bond strengths or examined any of the other factors that influence selectivity (solvent effects, kinetic factors, etc.). We can conclude, however, that the electronic structure of the Cm complexes with the heavier chalcogen donors is rather different from that of Eu and also Am. As noted above, Cm behaves very much as a trivalent ion with primarily ionic interactions with the ligands. Our data point to Eu and Am also having ionic metal−ligand bonds, although partial intramolecular charge transfer from the ligands to the metals generates larger f populations and significant divalent character. The longer bonds in the Eu and Am systems may well indicate weaker interactions than in the corresponding Cm complexes.

It is rather difficult, on the basis of the present results, to see how differences in f-based covalency between the middle of the lanthanide and actinide series can account for the soft-donor selectivity for the minor actinides over Eu; the f orbitals are too contracted to engage in covalent bonding. If the exploitation of covalency differences between actinide and lanthanide systems is deemed worthy of experimental pursuit, perhaps it should focus on potential differences in 5d/6d covalency? For both the six- and nine-coordinate target systems with the heavier chalcogens, the Am and Cm d populations are larger than those in the analogous Eu systems (Tables 7 and 8), although we note that there is no clear trend in these data for other An/Ln comparisons.

Finally, it is of interest to evaluate the extent to which La^{III}/U^{III} comparisons serve as good models for minor actinide/Eu systems. Our data suggest that using La^{III} and U^{III} as models for the middle of the f series is by no means perfect. The extent of f-based covalency is larger in the U complexes than anywhere else in the f block, and we believe it to be negligible for the minor actinides and Eu. The significant M^{II} tendencies of Eu and Am with the heavier chalcogens is not found for the earlier lanthanides and actinides, again raising questions as to the validity of La^{III}/U^{III} models. More data are required to probe these conclusions further and indeed to deepen our understanding of the changes in metal−ligand bonding as the 5f series is crossed. U frequently exhibits nontrivial f-based covalency in its complexes, by contrast to Cm, and further studies of the elements in between, and in particular Pu, are currently underway.

Acknowledgment. We are grateful to the EPSRC for Ph.D. studentships to K.I.M.I. and M.J.T. and for computing resources under Grant GR/S06233/01. We also thank the National Service for Computational Chemistry Software for allocations of time on its "Magellan" computing facility.

IC800835K

(34) Miguirditchian, M.; Guillaneux, D.; Guillaumont, D.; Moisy, P.; Madic, C.; Jensen, M. P.; Nash, K. L. *Inorg. Chem.* **2005**, *44*, 1404.
(35) Clark, A. E.; Sonnenberg, J. L.; Hay, P. J.; Martin, R. L. *J. Chem. Phys.* **2004**, *121*, 2563.